Techniques for Computing Fabric Tensors: A Review

Rodrigo Moreno, Magnus Borga, and Örjan Smedby

Abstract The aim of this chapter is to review different approaches that have been proposed to compute fabric tensors with emphasis on trabecular bone research. Fabric tensors aim at modeling through tensors both anisotropy and orientation of a material with respect to another one. Fabric tensors are widely used in fields such as trabecular bone research, mechanics of materials and geology. These tensors can be seen as semi-global measurements since they are computed in relatively large neighborhoods, which are assumed quasi-homogeneous. Many methods have been proposed to compute fabric tensors. We propose to classify fabric tensors into two categories: mechanics-based and morphology-based. The former computes fabric tensors from mechanical simulations, while the latter computes them by analyzing the morphology of the materials. In addition to pointing out advantages and drawbacks for each method, current trends and challenges in this field are also summarized.

1   Introduction

One of the ultimate goals of trabecular bone research in medicine is to determine the effect of pathological conditions of trabecular bone, such as osteoporosis and osteoarthritis, and their treatments on the quality of trabecular bone. One of the parameters that can be used to evaluate the bone quality is its anisotropy.

R. Moreno (✉) • Ö. Smedby
Department of Medical and Health Sciences (IMH), Center for Medical Image Science
and Visualization (CMIV), Linköping University, Campus US, 58185 Linköping, Sweden
e-mail: rodrigo.moreno@liu.se; orjan.smedby@liu.se

M. Borga
Department of Biomedical Engineering (IMT), Center for Medical Image Science
and Visualization (CMIV), Linköping University, Campus US, 58185 Linköping, Sweden
e-mail: magnus.borga@liu.se
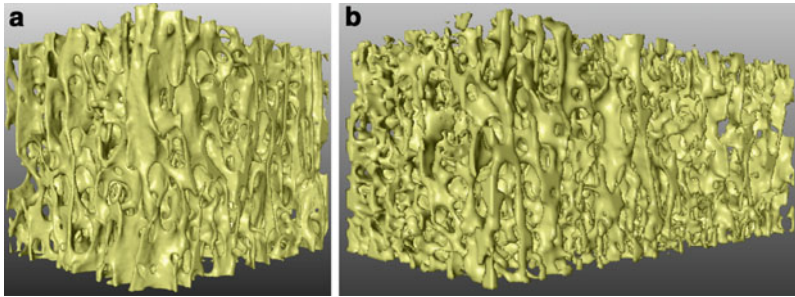
Fig. 1 Rendering of scans of trabecular bone from a radius and a vertebra respectively acquired through micro computed tomography

For example, evidences supporting that changes in the anisotropy and orientation of trabecular bone are associated with osteoporosis has been reported [11, 32, 47]. Figure 1 show renderings from two in vitro specimens.[1]

Trabecular bone is a tissue that is under continuous remodeling [57, 67, 68]. This remodeling process, which is driven by both physiology and mechanical adaptation processes, usually generates anisotropies in trabecular bone. Since mechanical stimuli differs from site to site of the body, analyses of changes over time of anisotropy generated by non-mechanical causes are performed site-dependent. In this context, fabric tensors are a fundamental tool to perform such kind of analyses.

Fabric tensors aim at modeling through tensors both anisotropy and orientation of a material of interest (usually referred to as *phase* in mechanics of materials) with respect to another one. In trabecular bone research, these two phases correspond to trabecular bone and bone marrow respectively. In addition to trabecular bone, fabric tensors have been used in other fields, such as mechanics of materials [91] and geology [49]. Fabric tensors are semi-global measurements in the sense that they are computed in relatively large neighborhoods, which are assumed quasi-homogeneous. In mechanics, such neighborhoods are usually referred to as representative volume elements (RVE) [72]. Furthermore, since it has been shown that microstructural architecture of most materials, including trabecular bone, can be accurately modeled by means of second-order tensors [48, 94], higher-order tensors are usually not computed.

In this context, the aim of this chapter is to review different approaches that have been proposed for computing fabric tensors, pointing out their advantages and disadvantages. We propose to classify these approaches into two categories: mechanics-based and morphology-based. The former approach computes fabric

---

[1]We thank Prof. Osman Ratib from the Service of Nuclear Medicine at the Geneva University Hospitals for providing the μCT scan of the vertebra; Andres Laib from SCANCO Medical AG and Torkel Brismar from the Division of Radiology at the Karolinska University Hospital for providing the μCT scan of the radius.

tensors from mechanical simulations, while the latter computes them by analyzing the morphology of trabecular bone. It is important to remark that, although some authors do not consider tensors computed through mechanical simulations as a specific type of fabric tensors, we argue they actually are fabric tensors, since they can also be used to describe orientation and anisotropy of trabecular bone, which is the main purpose of fabric tensors. Invariably, the input of all methods is an RVE and the output is the fabric tensor associated to it.

The chapter is organized as follows. The next two sections review the most important methods that follow the aforementioned approaches. Section 4 reviews the research to relate fabric tensors computed through morphology analyses and mechanical properties of the bone. Finally, Sect. 5 makes some concluding remarks, focusing on the current topics in fabric tensors research. As a convention, scalars, vectors and tensors are written in italic, bold and straight font respectively in the paper, e.g. λ, $\mathbf{p}$ and VO.

2 Mechanics-Based Methods

The most relevant property of trabecular bone is its mechanical competence, that is, its capability to bear different types of mechanical loads in different orientations. In this line, mechanics-based methods directly measure fabric tensors from mechanical properties. Since it is difficult to conduct reliable mechanical experiments, these methods compute the tensors through numerical simulations. The next subsections summarize some approaches that follow this path.

2.1 Solid Mechanics Approach

This approach makes use of solid mechanics. A common simplification is to assume that trabecular bone is an elastic material [73]. Thus, under linearity conditions, the so-called stiffness (or elasticity) tensor can directly be used as a fabric tensor. By using the Einstein summation convention, which means that repeated indices imply a summation over them, the stiffness tensor c, can be written as:

$$\sigma_{ij} = \mathsf{c}_{ijk\ell}\,\epsilon_{k\ell}, \tag{1}$$

where σ and ϵ are the stress and strain tensors respectively. Notice that σ and ϵ are of second-order, while c is of fourth-order. This equation corresponds to the generalization of the Hooke's law. Thanks to the symmetries of σ and ϵ, c only has 21 out of 81 independent terms. Assuming orthotropic symmetry of trabecular bone [100] the number of independent can be further reduced to nine. By using the Voigt notation [29], c can be represented by the following 6×6 symmetric second-order tensor:

$$\hat{c} = \begin{pmatrix} c_{1111} & c_{1122} & c_{1133} & \sqrt{2}c_{1123} & \sqrt{2}c_{1113} & \sqrt{2}c_{1112} \\ c_{1122} & c_{2222} & c_{2233} & \sqrt{2}c_{2223} & \sqrt{2}c_{2213} & \sqrt{2}c_{2212} \\ c_{1133} & c_{2233} & c_{3333} & \sqrt{2}c_{3323} & \sqrt{2}c_{3313} & \sqrt{2}c_{3312} \\ \sqrt{2}c_{1123} & \sqrt{2}c_{2223} & \sqrt{2}c_{3323} & 2c_{2323} & 2c_{2313} & 2c_{2312} \\ \sqrt{2}c_{1113} & \sqrt{2}c_{2213} & \sqrt{2}c_{3313} & 2c_{2313} & 2c_{1313} & 2c_{1312} \\ \sqrt{2}c_{1112} & \sqrt{2}c_{2212} & \sqrt{2}c_{3312} & 2c_{2312} & 2c_{1312} & 2c_{1212} \end{pmatrix} \qquad (2)$$

The entries of stiffness tensors computed at a local scale can be estimated by running several finite element method (FEM) simulations, at least six [80], each of them with a different boundary condition. Once the local stiffness tensors have been computed, a homogenization procedure can be applied in order to obtain from local estimations a single effective stiffness tensor representative for the whole representative volume element. It has been shown that component-wise addition is not a valid strategy to perform such a homogenization. Thus, more advanced homogenization techniques are usually applied. For example, local structure tensors computed from the relation between local and global strains can be used to steer the homogenization process [9, 30, 31, 80]. Alternatively, Riemannian metrics and the Kullback-Leibler divergence can be applied to aggregate the local tensors [61].

Computing the stiffness tensor through FEM simulations is still under active research [34, 73, 78]. One of the most important problems faced by researchers is that the results can have a large variation for the same sample by applying different boundary conditions, homogenization schemes and methods to generate nodes for the FEM simulations. In addition, another source of error is that the computations are based on the aforementioned simplifications that can be inaccurate. For example, it is well-known that trabecular bone is much better resisting compression than tension [16], while the computed stiffness tensor will predict the same behavior under both boundary conditions. Moreover, most methods are restricted to images acquired from in vitro specimens, as images acquired in vivo have very low quality, which difficults the segmentation required by FEM simulations [40].

2.2 Wave Propagation Approach

A more recent approach use FEM simulations of wave propagation on trabecular bone to describe orientation and anisotropy of trabecular bone. Assuming a poroelastic behavior, it has been shown that wave propagation on trabecular bone can be characterized through the acoustic tensor, Q, the solid-fluid interaction tensor, C, and the intrinsic permeability tensor, K, which describe the elastic and viscous effects on the media [14, 15]. Q and C are second-order tensors that are related to the Biot's parameters that describe the stress-strain relation in porous media [12] and the exciting waves. In turn, K, a second-order tensor derived from Darcy's law, takes into account dissipation due to viscous losses and it is closely related to the

tortuosity tensor [76]. A close relation between these tensors and morphology-based fabric tensors has been reported [14].

A shortcoming of this approach is that simulated acoustical properties of trabecular bone have a non-linear dependence on the composition of bone marrow and bone volume fraction, as well as on the resolution of the images [2]. As well as solid mechanics approaches, wave propagation simulations are restricted to high resolution images acquired from in vitro specimens, making it difficult its use in clinical practice.

3 Morphology-Based Methods

Methods that follow this approach compute fabric tensors from the morphology of trabecular bone. These methods have two advantages compared to the methods described in Sect. 2. First, they are largely less computationally expensive than those obtained from mechanical simulations. Second, unlike methods based on mechanics, the resulting fabric tensors are not dependent on the boundary conditions applied during the simulations, homogenization schemes and/or general design of the simulations. However, as a counterpart, it is necessary to relate these fabric tensors with mechanical properties of the material, especially, elasticity.

The vast majority of morphology-based methods use specific features to estimate orientation distributions which are approximated through fabric tensors. If the estimation is performed locally, a homogenization process is applied (usually tensorial summation) in order to obtain global measurements of orientation and anisotropy. The next subsections describe the most important families of methods that follow this approach, which are summarized in Table 1.

3.1 Boundary-Based Methods

Boundary-based methods use the interface between phases to estimate fabric tensors. The Mean Intercept Length tensor (MIL) [83, 94] and the global gradient structure tensor (GST) [6, 88] belong to this category.

3.1.1 Mean Intercept Length Tensor

In trabecular bone research, the MIL tensor is considered as the gold standard thanks to the large amount of evidence supporting its appropriateness to predict mechanical properties of trabecular bone [16, 60, 70, 103]. The MIL tensor was originally proposed as a sampling procedure taken from stereology [83, 94]. The MIL with respect to a particular orientation is defined as the mean distance between a change from one phase to the other in such an orientation. This value

Table 1 Summary of morphology-based methods

Approach	Method
Boundary-based	Mean Intercept Length (MIL) tensor [64, 83, 94]
	Generalized MIL tensor [64]
	Global gradient structure tensor (GST)[6, 59, 88]
Volume-based	Volume orientation tensor (VO) [70]
	Star volume distribution (SVD) [70]
	Star length distribution (SLD) [70]
	Tensor scale [52, 82, 99]
	Inertia tensor [35, 90]
	Sampling sphere orientation distribution (SSOD) [89]
Texture-based	Fractal dimension (FD) [5, 26, 55, 59, 102]
	Hurst orientation transform [77]
	Variance orientation transform [97, 98]
	Line fraction deviation [20, 21]
	Spatial autocorrelation [92]
	Different statistics [27]
Alternative methods	Minkowski tensors [84, 85]
	Diffusion tensor imaging (DTI) [8, 81]
	Texture tensor [23]
	Skeleton-driven [41]
	Assessment of the power spectrum [7]

Fig. 2 Computation of the intercepts between a set of parallel lines and the interface between phases. In this example, the number of intercepts is 13
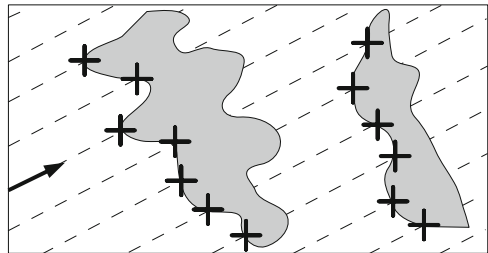
is inversely proportional to the number of intercepts between a set of parallel lines and the interface between phases (see Fig. 2). The MIL tensor is obtained either by applying ellipse/ellipsoid fitting algorithms to polar plots of the MIL computed in different orientations, also known as rose diagrams, or by computing a covariance matrix [38, 64, 87]. Although the orientation distribution of the MIL can also be approximated through higher-order fabric tensors [38], microstructural architecture of most materials can be accurately modeled by means of second-order tensors [48, 94].

Recently, we have proposed a closed formulation for computing the MIL tensor [64]. We have shown that the orientation distribution of intercepts, C_{MIL}, is proportional to the angular convolution between the mirrored extended Gaussian image [33], G, of the sample and the half-cosine kernel, K, which is given by:

$$K(\phi) = \begin{cases} \cos(\phi) \ if \phi \le \pi/2 \\ 0 \quad otherwise. \end{cases} \tag{3}$$

Thus, C_{MIL} can be computed through:

$$C_{MIL} = \alpha \, G * K, \tag{4}$$

where α is a constant and "$*$" is the angular convolution. Finally, the MIL tensor can be computed by computing a covariance matrix on $1/C_{MIL}$.

This formulation solves several problems of sampling procedures. First, since sampling is avoided, the accuracy is not any longer dependent on the computational cost of the implementation. Second, the new method is not exposed to discretization artifacts generated by line-drawing algorithms. Third, the new formulation is inexpensive since, thanks to the Funk-Hecke theorem [25], the angular convolution can efficiently be computed in the spherical harmonics domain. Fourth, robust implementations of the MIL tensor can straightforwardly be obtained from robust estimations of the extended Gaussian image. Fifth, the new formulation makes straightforward the extension of the MIL tensor to non-binarized images. Finally, the MIL tensor can be generalized by changing different convolution kernels, e.g. to powers of the half-cosine function or the von Mises-Fisher kernel [37].

3.1.2 Global Gradient Structure Tensor

Another boundary-based fabric tensor is the GST [6, 59, 88]. For an image I, the GST is computed as:

$$\mathsf{GST} = \int_{\mathbf{p} \in I} \nabla \mathbf{I_p} \nabla \mathbf{I_p}^T \, dI. \tag{5}$$

Notice that the GST is related to the traditional local structure tensor (ST) [19] computed with a Gaussian of zero mean and standard deviation ρ, K_ρ. If the size of the image is much larger than ρ, the GST can be written as:

$$\mathsf{GST} = \int_{\mathbf{p} \in I} \mathsf{ST} \, dI = \int_{\mathbf{p} \in I} (K_\rho * \nabla \mathbf{I_p} \nabla \mathbf{I_p}^T) \, dI. \tag{6}$$

This method has two interesting properties. First, implementations of the GST are efficient, both in the spatial and frequency domains, and easy to code. Second, the GST and the MIL share the same eigenvectors for binary images [64]. Basically, the GST can be computed as the covariance matrix of $C_{GST} = G * \delta$, where δ is the unit impulse function and G is the mirrored extended Gaussian image. Thus, the difference between the MIL tensor and the GST is that they use a different convolution kernel for computing functions C_{MIL} and C_{GST} and the former calculates the covariance matrix on $1/C_{MIL}$ while the latter on C_{GST}. Hence, both tensors will

Fig. 3 Example of a material
in which boundary-based
tensors are unable to estimate
anisotropy and orientation.
Both, the MIL and GST
tensors are isotropic in this
case
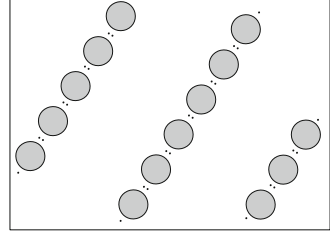
share the eigenvectors, since both the unit impulse function and the half-cosine
kernel are positive and symmetric and changing C by its inverse in the computations
does not introduce rotations in the eigenvectors [25].

As an alternative, global structure tensors can also be estimated from local
structure tensors computed through quadrature filters [24, 44, 45], by using higher-
order derivatives [18, 46] or by means of tensor voting [66].

A drawback of this technique is that the eigenvalues are different to those from
the MIL tensor, and the larger one is perpendicular to the main orientation of
trabecular bone [88, 96]. Consequently, anisotropies computed through the GST are
expected to be in less agreement with the anisotropies yielded by the stiffness tensor
[65]. This means that, in practice, the resulting tensor has to be post-processed in
order to be used as a predictor of mechanical properties.

3.2 Volume-Based Methods

A problem of the boundary-based methods is that they are only appropriate where
the anisotropy and orientation are determined by the interface between phases. For
example, boundary-based methods are unable to estimate anisotropy in the case of
Fig. 3.

To solve this issue, volume-based methods compute anisotropy from measures
taken inside one of the phases. The next subsections describe the most important
families of methods that follow this approach.

3.2.1 Distributions of Intercepting Lines

There are many fabric tensors that are computed through the sampling procedure
shown in Fig. 4. First, a set of N sampling points are generated in the material of
interest (e.g., trabecular bone). Second, the intercept length of lines with different
orientations that cross every testing point is computed.

Several features can be extracted in order to compute fabric tensors. For example,
local volume orientation at a point is given by the orientation corresponding to
the largest intercept at that point. The volume orientation tensor VO, is computed
as [70]:
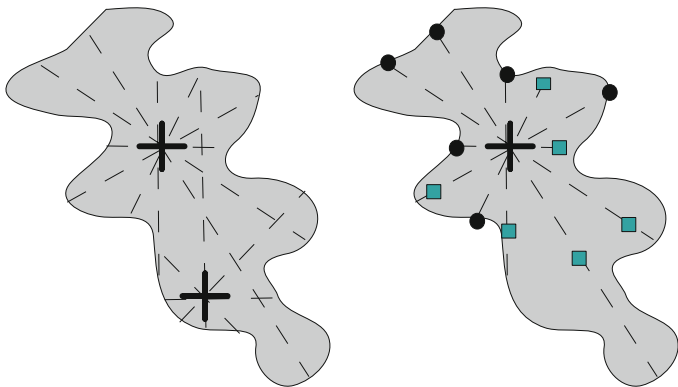
Fig. 4 Distributions of intercepting lines. *Left*: lines with different orientations are traced from some sampling points (marked with *crosses*). The lenght of those lines are used to generate the VO, SVD and SLD tensors. *Right*: in order to compute the scale tensor, line segments are shortened (half of the intercepts with the boundary are shifted to the positions marked with *squares*) in order to make them symmetric with respect to the sampling point

$$\mathsf{VO} = \sum_{i=1}^{N} L_{max_i} \; \mathbf{v}_{max_i} \; \mathbf{v}_{max_i}^{T}, \tag{7}$$

where L_{max_i} and $\mathbf{v}_{max_i}$ are the largest intercept at i and its corresponding orientation respectively. On the other hand, the star volume (SVD) and length distributions (SLD) consider all intercepts, not only the maximum for computing the fabric tensor. They are computed as:

$$\mathsf{SVD} = \int_{\mathbf{v} \in \Omega} \left(\sum_{i=1}^{N} L_i^3(\mathbf{v}) \; \mathbf{v} \mathbf{v}^{T} \right) d\Omega, \tag{8}$$

$$\mathsf{SLD} = \int_{\mathbf{v} \in \Omega} \left(\sum_{i=1}^{N} L_i(\mathbf{v}) \; \mathbf{v} \mathbf{v}^{T} \right) d\Omega, \tag{9}$$

where Ω is the unitary sphere, and $L_i(\mathbf{v})$ is the intercept at i with respect to the orientation $\mathbf{v}$. Thus, the main difference between SVD and SLD is the power of L used in the formulation.

A related fabric tensor is the tensor scale [82, 99]. In this case, every intercepting segment is symmetrized with respect to the reference point by replicating the closest length to the edge in the opposite direction. A local tensor at the sampling positions is computed with the length of the symmetrized lines and the final fabric tensor is computed by adding all local tensors.

In [71] is reported that SVD and SLD are better predictors of mechanical orientation. However, the same study also reports that the MIL is a better predictor

of mechanical anisotropy. Regarding the tensor scale, an initial study reported good correlations between this tensor and mechanical properties [52].

The most important drawback of the methods presented in this subsection is their computational cost. Since these methods are based on a sampling procedure, the accuracy of the computations is related to the complexity of the algorithms. Usually, a huge amount of tests is required to obtain a reasonable accuracy.

3.2.2 Inertia-Based Methods

An straightforward way to compute a volume-based fabric tensor is to compute a global inertia tensor [35] of the material of interest, which is given by:

$$\mathsf{IT} = \int_{\mathbf{x} \in I} \rho(\mathbf{x}) \left((\mathbf{x} - \mathbf{s})^2 \, \mathsf{I} - (\mathbf{x} - \mathbf{s})(\mathbf{x} - \mathbf{s})^T \right) \, dI \tag{10}$$

where I is the image, $\rho(\mathbf{x})$ is the gray-scale value at $\mathbf{x}$, which is assumed to be proportional to the mass at that point, and $\mathbf{s}$ is the center of mass. However, poor correlations with the MIL tensor have been reported [96], and consequently, it is expected to be a bad predictor of mechanical properties. A possible hypothesis for this is that the path that joins every position to the center of mass usually includes large regions of bone marrow and this fact can influence its appropriateness as fabric tensor.

A possible way to tackle this problem is to compute local inertia tensors computed in local spherical neighborhoods, as proposed in [90], and then to generate a global inertia tensor by adding them up or using any other homogenization scheme. A related strategy is the sampling sphere orientation distribution [89], which adds the gray-scale values of spherical neighborhoods located at some specific sampling locations into a spherical container, as shown in Fig. 5. These neighborhoods are chosen in such a way that their centers are as close as possible to the skeleton of the material of interest. The resulting container is approximated through tensors following an adapted version of the technique proposed in [38]. Since these approximations are related to the computation of the inertia tensor in the container, the method can be seen as a homogenization scheme for computing a global inertia tensor from local inertia information. From the results presented in [89], the use of local inertia tensors partially solves the problems of the global inertia tensor, since the resulting tensors are more correlated with the MIL tensor.

3.3 Texture-Based Methods

The following subsections describe some methods that make use of texture analysis tools to compute fabric tensors.
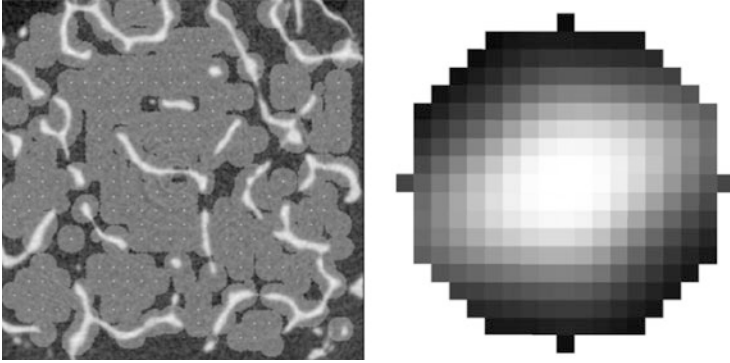
Fig. 5 SSOD. *Left*: the image is sampled with some spheres. *Right*: the gray-scale values are accumulated in a spherical container. Fabric tensors approximate the gray-scale values in the container (Reprinted from [89] with permission from Elsevier)

3.3.1 Fractal-Based Methods

These methods assume a fractal nature of trabecular bone. The basic idea of this approach is to perform directional measurements of fractal dimension (FD) to create orientation distributions that, afterwards, are approximated through tensors. The FD can be computed in many different ways [54]. A basic strategy is the so-called box-counting algorithm where FD is estimated as:

$$\text{FD} = -\lim_{r \to 0} \frac{\log N(r)}{\log(r)} \tag{11}$$

where r is the size of a box and $N(r)$ is the number of boxes required to utterly cover the material of interest. Similar to this method are the skyscrapers and blanket fractal analyses [26].

Alternatively, by assuming a fractional Brownian motion model [5], FD can be computed in the Fourier domain for a specific direction as a function of the slope of the linear regression computed on a log-log plot of the power spectrum vs. frequency [55, 59, 75, 102]. The process is shown in Fig. 6 for a specific orientation.

Since very often this log-log curve does not have a linear behavior for the whole spectrum, it is common to use two fitting lines: for low and high frequencies respectively [55] (see Fig. 6). Some other methods to compute the FD are the augmented Hurst orientation transform [77] and the variance orientation transform [97, 98].

Most of these methods perform the computations in the Fourier domain. Since measurements are performed at specific directions, it is more convenient to sample the Fourier domain by using polar or spherical coordinates instead of Cartesian. However, computing fast Fourier transform in polar/spherical coordinates is not yet a mature technique, although important advances have been done in the last few years [3, 39, 93].
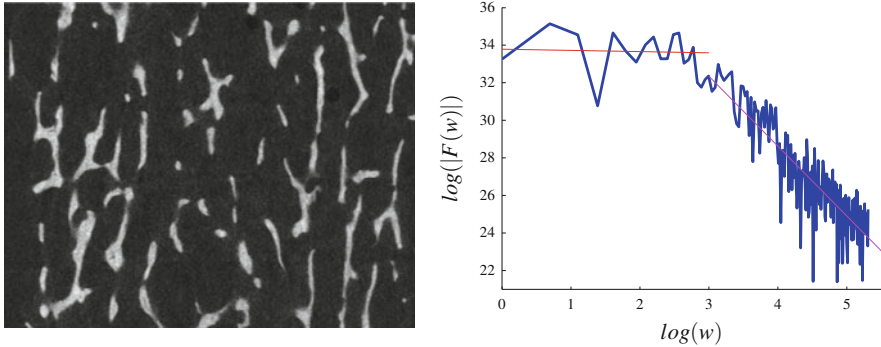
Fig. 6 Estimation of the FD. *Left*: a 2D slice of the image of Fig. 1a. *Right*: log-log plot of the power spectrum vs. frequency at a specific orientation and two linear regressions covering low and high frequencies respectively

A drawback of fractal-based methods is that it is still not clear whether or not trabecular bone follows a fractal pattern with authors in favor [74] and against this hypothesis [10]. From our own experience, the required computation of linear regressions usually involves large errors for images of trabecular bone. As a consequence, since these errors have a direct impact in the computation of fabric tensors, that makes it difficult to obtain reliable and accurate results. Despite this, good correlations with mechanical properties have been reported [55]. Another drawback is that, although the methods can be extended to 3D, they have usually been tested in 2D images of trabecular bone.

3.3.2 Texture Features

Some authors have proposed directional texture features to compute fabric tensors. For example, the line fraction deviation method [20] constructs an orientation distribution from the variance of the gray-scale values along test lines at different orientations, which is then approximated through tensors. Good correlations with the stiffness tensor have been reported for this method [21]. The basic ideas of this method are related to the variance orientation transform from fractal analysis [97, 98].

Related to this strategy, in [92],spatial autocorrelation of the gray-scale values instead of the variance is used to construct the orientation distribution. Their main assumption is that trabecular bone has a quasi-regular structure. However, in [86] is reported that the resulting fabric tensor does not correlate with mechanical properties of trabecular bone. Alternatively, other statistical measurements can be used instead of the variance or spatial autocorrelation to construct the orientation distribution [27].

3.4 Alternative Methods

Recently, the Minkowski tensors have been proposed as an elegant a way to integrate boundary- and volume-based techniques [84, 85]. Six linearly independent Minkowski tensors are defined in 3D:

$$W_0^{2,0} = \int_{\mathbf{p} \in V} \mathbf{p}\,\mathbf{p}^T \, dV, \tag{12}$$

$$W_1^{2,0} = \frac{1}{3} \int_{\mathbf{p} \in S} \mathbf{p}\,\mathbf{p}^T \, dS, \tag{13}$$

$$W_2^{2,0} = \frac{1}{3} \int_{\mathbf{p} \in S} H(\mathbf{p})\,\mathbf{p}\,\mathbf{p}^T \, dS, \tag{14}$$

$$W_3^{2,0} = \frac{1}{3} \int_{\mathbf{p} \in S} G(\mathbf{p})\,\mathbf{p}\,\mathbf{p}^T \, dS, \tag{15}$$

$$W_1^{0,2} = \frac{1}{3} \int_{\mathbf{p} \in S} \mathbf{n}\,\mathbf{n}^T \, dS, \tag{16}$$

$$W_2^{0,2} = \frac{1}{3} \int_{\mathbf{p} \in S} H(\mathbf{p})\,\mathbf{n}\,\mathbf{n}^T \, dS, \tag{17}$$

where $\mathbf{p}$ represents the position of points inside the trabecular bone, V, $\mathbf{n}$ is the normal at $\mathbf{p}$ at the interface between phases, S, and $H(\mathbf{p})$ and $G(\mathbf{p})$ are the mean and Gaussian curvatures at $\mathbf{p}$ respectively. These tensors are called the moment tensor solid, moment tensor hollow, moment tensor wireframe, moment tensor vertices, normal distribution and curvature distribution tensors respectively [85]. Notice that the moment tensor solid and the normal distribution tensor are closely related to the inertia tensor and the GST respectively. Afterwards, different measurement of orientation and anisotropy can be obtained from these six tensors.

Since marrow contains large amounts of water, a promising alternative method to estimate fabric tensors experimentally is through diffusion tensor imaging (DTI) [8, 56, 81]. Although DTI has extensively been used in fiber tractography (see other chapters of this book), its use in trabecular bone is relatively scarce. The following reasons have impeded a faster development of this approach. First, this method computes orientation and anisotropy of bone marrow instead of trabecular bone, so the resulting tensor must conveniently be post-processed in order to obtain a fabric tensor of trabecular bone, and, to our knowledge, such a post-processing has not been proposed so far. Second, it necessary to develop new DTI pulse sequences, since the ones used for white matter in the brain are not appropriate for bone marrow as these two types of tissue have very different magnetic properties and morphology.

A technique used in research of foamy structures is the so-called texture tensor [23]. Given a lattice or mesh, a local texture tensor is computed by aggregating tensorized vectors (i.e. the outer product of these vectors with themselves) that

connect the center of a cell with the centers of neighboring cells. A global texture tensor is then computed by aggregating local texture tensors. A drawback of this technique when it is applied to trabecular bone is that the resulting tensor will depend on the technique used to generate the required input mesh.

An alternative way to construct orientation distributions from the skeleton of trabecular bone was proposed in [41], where mass and thickness of every branch in the skeleton is associated to its orientation. The main drawback of this approach is that it assumes that trabecular bone is composed by rod-like trabeculae, which largely limits its scope of use as it has been shown that this assumption is not always complied [63].

Finally, in [7] anisotropy is directly extracted from a visual examination of the power spectrum of X-ray images. Unlike all methods reviewed in this chapter, this technique is biased by the human observer's perception and, in practice, it can only be used for very anisotropic structures.

4   Relations Between Morphology-Based Fabric Tensors and Mechanics

Morphology-based methods are appealing since they do not have any dependency on boundary conditions, and consequently they are more predictable. However, unlike mechanics-based, morphology-based methods require an extra step of validation with respect to mechanical properties of the tissue, since the quality of a fabric tensor is given by its capacity of predicting mechanical properties in realistic scenarios. Usually, this assessment is performed with respect to a model [103]. A complete review of the models proposed in the literature is presented in [103]. For illustration, two of such models are presented below.

Let $\otimes$ and $\overline{\overline{\otimes}}$ be the tensorial and double tensorial products of second-order tensors respectively, which, using the Einstein summation notation, are given by [104]:

$$\mathsf{A} \otimes \mathsf{B} = \mathsf{A}_{ik}\mathsf{B}_{jl}, \tag{18}$$

$$\mathsf{A} \overline{\overline{\otimes}} \mathsf{B} = \frac{1}{2}(\mathsf{A}_{ik}\mathsf{B}_{jl} + \mathsf{A}_{il}\mathsf{B}_{jk}). \tag{19}$$

On the one hand, Cowin [13] proposed that the stiffness c and a fabric tensor M should be related through the formula:

$$\mathsf{c}(\nu, \mathsf{M}) = \sum_{a,b=1}^{3} (\lambda_{ab}(\nu, m_a, m_b)\mathsf{M}_a \otimes \mathsf{M}_b) + \sum_{a,b=1, a \neq b}^{3} 2(\mu_{ab}(\nu, \mathbf{m}_a, \mathbf{m}_b)\mathsf{M}_a \overline{\overline{\otimes}} \mathsf{M}_b), \tag{20}$$

where ν is the volume fraction, m_a and $\mathbf{m}_a$ are the eigenvalues and eigenvectors of the fabric tensor M respectively, $\mathsf{M}_a = \mathbf{m}_a \mathbf{m}_a^T$, λ_{ab} and μ_{ab} are unknown functions of ν, m_a and m_b,

Alternatively, the following stiffness-fabric relation was proposed by Zysset and Curnier [104]:

$$\mathsf{c}(\nu, \mathsf{M}) = \sum_{a,b=1}^{3} ((\lambda_0 + 2\mu_0)\nu^\alpha m_a^\beta m_b^\beta \mathsf{M}_a \otimes \mathsf{M}_a) + \sum_{a,b=1,a\neq b}^{3} (2\mu_0 \nu^\alpha m_a^\beta m_b^\beta \mathsf{M}_a \overline{\underline{\otimes}} \mathsf{M}_b)$$

(21)

where α and β are constants and λ_0 and μ_0 are the unknown functions.

Once a model is chosen, multilinear regressions are performed in order to estimate the unknown functions (λ_{ab} and μ_{ab} for Cowin's model, or λ_0 and μ_0 for Zysset and Curnier's model) that minimizes the error between the actual stiffness tensor and the one estimated with the model. The reference stiffness tensor can be estimated either through mechanical simulations as described in Sect. 2.1, or through mechanical experiments [103]. Thus, a morphology-based fabric tensor with a small error between the actual and estimated stiffness tensor is preferred, since this indicates that it is more related to mechanical properties of the tissue.

The MIL tensor usually has the better performance in these assessments. An interesting alternative to minimize the error between the reference and estimated stiffness tensor is to include parameters in the computation of the fabric tensor, as we proposed in [64]. This can give more flexibility to the fitting process, resulting in better estimations of the reference stiffness tensor.

Assessing relations between fabric tensors and mechanical properties of trabecular bone is far from easy. First, these comparisons are mainly restricted to in vitro where the reference stiffness tensor can be obtained. On the one hand, it is difficult to compute reliable stiffness tensors from mechanical simulations from low-resolution images. However, the high-resolution images needed for mechanical simulations are not attainable in vivo for practical and radiation protection issues. On the other hand, invasive mechanical measurements in vivo are not reliable, since they are based on many assumptions. Moreover, such measurements and not always possible for every skeletal site [69, 101].

Reference stiffness tensors obtained through mechanical experiments are preferred to those obtained from mechanical simulations as they are more closely related to reality and do not have the aforementioned problems of mechanical simulations. Unfortunately, it is also difficult to design reliable mechanical experiments in vitro. On the one hand, these experiments are exposed to several sources of error [70, 73]. On the other hand, measurements are usually available in only a few directions (very often in a single one), so many experiments have to be conducted for different directions in order to be combined afterwards, a procedure that is prone to errors. Moreover, it is usually unknown the relationship between the main orientation of trabecular bone and the tested orientations.

For these difficulties, many authors validate their methods by making comparisons with the MIL tensor instead of with the stiffness tensor. However, a direct relationship between a new method and the stiffness tensor is necessary when a better performance than the MIL tensor is being reported.

5 Concluding Remarks

This chapter has presented a comprehensive review of techniques for computing fabric tensors. In general, current methods tend to be less manual and more accurate by addressing most of the disadvantages from previous approaches. Despite this, research in fabric tensors is far from mature and many issues need to be tackled.

First, image acquisition of trabecular bone is challenging in vivo due to the size of the trabecular structure. For example, trabecular thickness ranges between 100 and 300 μm depending on the skeletal site [62], while standard magentic resonance imaging (MRI) and computed tomography (CT) scanners offer resolutions of about 500 and 100 μm respectively. That means that a complete trabecula is covered by at most three voxels, making these images prone to partial volume effects. In addition, blurring, artifacts and noise are not uncommon in these type of images. Hence, it is difficult to perform accurate morphological analyses in vivo. For this reason, methods for computing fabric tensors in gray-scale are appealing, since they are not affected by the accuracy of the segmentation process, which is particularly difficult for images acquired in vivo. Also, the quality of the images are expected to be improved in the next few years, especially with high-resolution peripheral quantitative computed tomography (HR-pQCT) and cone beam computed tomography (CBCT) scanners, which are able to obtain spatial resolutions in the order of 80 μm in vivo [4,43] with very low radiation doses, which can range between 3 and 10 μSv for HR-pQCT [17] and between 11 and 77 μSv for CBCT [53] compared to the 3 mSv usually required by high-resolution multi-detector CT (HR-MDCT) scanners. It is important to remark that, in clinical practice, physicians use dual-energy X-ray absorptiometry (DXA) for measuring the bone mineral density. However, this technique is unable to measure differences in the trabecular structure, which has been shown more related to the development of trabecular bone diseases [42]. Other in vivo techniques such as quantitative ultrasound (QUS) [28, 79] and resonance frequency analyzers (RFA) [1, 58] face the same problematic as DXA.

Second, it is important to remark that fabric tensors are not global measurements. Thus, it is possible to obtain fields of fabric tensors where tensors are computed locally with respect to a neighborhood. However, large neighborhoods are usually used, since regions of interest are usually assumed homogeneous. The net result of this is that the resulting tensor field varies slowly in the space. In consequence, a single tensor is usually computed as a representative measurements for a complete region of interest. However, homogeneity for trabecular bone analysis has been questioned by some authors, e.g., [72]. This imposes the problem of determining the appropriate size of neighborhoods. One strategy to tackle this issue is to propose

measurements of homogeneity of neighborhoods. Regarding fabric tensors, an alternative is to assess changes in orientation and anisotropy with respect to the size of the neighborhood used in the computations. To our knowledge, these types of analysis have not been proposed so far.

Third, some authors argue that it is not necessary to perform measurements in 3D, since features extracted from 3D and 2D projections have been shown correlated [36, 95]. However, this point requires more extensive validation with different features and skeletal sites.

Finally, some authors have found that higher-order tensors are necessary at some skeletal sites, e.g. the calcaneus [21, 22]. This should not be a big problem for most methods, since they usually compute orientation distributions that are approximated through tensors, which can be in theory of any kind. Moreover, methods for performing such approximations are well-established [38, 50, 51]. Despite this, an extensive validation of this point is necessary. On the other hand, it is necessary to bear in mind that, assuming linearity, fourth-order would be the highest necessary order for any fabric tensor, since that is the order of the stiffness tensor. Alternatively, other approximation methods can be used instead of tensors in order to model orientation distributions, e.g., spherical harmonics [41].

To summarize, despite large amount of work in the field, and the advances attained in last decades, there are still many unsolved issues in order to use fabric tensors in clinical practice of trabecular bone diseases. We think proposals to tackle these issues will steer the research in the field in the oncoming years.

References

1. Abtahi, J., Tengvall, P., Aspenberg, P.: A bisphosphonate-coating improves the fixation of metal implants in human bone. a randomized trial of dental implants. Bone **50**(5), 1148–1151 (2012)
2. Aula, A., Töyräs, J., Hakulinen, M., Jurvelin, J.: Effect of bone marrow on acoustic properties of trabecular bone – 3d finite difference modeling study. Ultrasound Med. Biol. **35**(2), 308–318 (2009)
3. Averbuch, A., Coifman, R., Donoho, D., Elad, M., Israeli, M.: Fast and accurate polar Fourier transform. Appl. Comput. Harmon. Anal. **21**(2), 145–167 (2006)
4. Bauer, J.S., Link, T.M.: Advances in osteoporosis imaging. Eur. J. Radiol. **71**(3), 440–449 (2009)
5. Benhamou, C.L., Lespessailles, E., Jacquet, G., Harba, R., Jennane, R., Loussot, T., Tourliere, D., Ohley, W.: Fractal organization of trabecular bone images on calcaneus radiographs. J. Bone. Miner. Res. **9**(12), 1909–1918 (1994)
6. Bigün, J., Granlund, G.H.: Optimal orientation detection of linear symmetry. In: Proceedings of the International Conference on Computer Vision (ICCV), London, pp. 433–438 (1987)
7. Brunet-Imbault, B., Lemineur, G., Chappard, C., Harba, R., Benhamou, C.L.: A new anisotropy index on trabecular bone radiographic images using the fast Fourier transform. BMC Med. Imaging **5**, 4 (2005)
8. Capuani, S., Rossi, C., Alesiani, M., Maraviglia, B.: Diffusion tensor imaging to study anisotropy in a particular porous system: the trabecular bone network. Solid State Nucl. Magn. Reson. **28**(2–4), 266–272 (2005)

9. Charalambakis, N.: Homogenization techniques and micromechanics. A survey and perspectives. Appl. Mech. Rev. **63**, 030,803–1–030,803–10 (2010)
10. Chung, H.W., Chu, C.C., Underweiser, M., Wehrli, F.W.: On the fractal nature of trabecular structure. Med. Phys. **21**(10), 1535–1540 (1994)
11. Ciarelli, T.E., Fyhrie, D.P., Schaffler, M.B., Goldstein, S.A.: Variations in three-dimensional cancellous bone architecture of the proximal femur in female hip fractures and in controls. J. Bone Miner. Res. **15**(1), 32–40 (2000)
12. Coussy, O.: Poromechanics, 2nd edn. Wiley, Chichester (2004)
13. Cowin, S.: The relationship between the elasticity tensor and the fabric tensor. Mech. Mater. **4**(2), 137–147 (1985)
14. Cowin, S.C., Cardoso, L.: Fabric dependence of bone ultrasound. Acta Bioeng. Biomech. **12**(2), 3–23 (2010)
15. Cowin, S.C., Cardoso, L.: Fabric dependence of wave propagation in anisotropic porous media. Biomech. Model Mechanobiol. **10**(1), 39–65 (2011)
16. Cowin, S.C., Doty, S.B.: Tissue Mechanics. Springer, New York (2007)
17. Damilakis, J., Adams, J.E., Guglielmi, G., Link, T.M.: Radiation exposure in X-ray-based imaging techniques used in osteoporosis. Eur. Radiol. **20**(11), 2707–2714 (2010)
18. Felsberg, M., Jonsson, E.: Energy tensors: Quadratic, phase invariant image operators. In: Proceedings of the Symposium German Association for Pattern Recognition (DAGM), Vienna. Lecture Notes in Computer Science, vol. 3663, pp. 493–500 (2005)
19. Förstner, W.: A feature based correspondence algorithm for image matching. Int. Arch. Photogramm. Remote Sens. **26**, 150–166 (1986)
20. Geraets, W.G.: Comparison of two methods for measuring orientation. Bone **23**(4), 383–388 (1998)
21. Geraets, W.G.M., van Ruijven, L.J., Verheij, J.G.C., van der Stelt, P.F., van Eijden, T.M.G.J.: Spatial orientation in bone samples and young's modulus. J. Biomech. **41**(10), 2206–2210 (2008)
22. Gomberg, B.R., Saha, P.K., Wehrli, F.W.: Topology-based orientation analysis of trabecular bone networks. Med. Phys. **30**(2), 158–168 (2003)
23. Graner, F., Dollet, B., Raufaste, C., Marmottant, P.: Discrete rearranging disordered patterns, part I: robust statistical tools in two or three dimensions. Eur. Phys. J. E: Soft Matter Biol. Phys. **25**(4), 349–369 (2008)
24. Granlund, G.H., Knutsson, H.: Signal Processing for Computer Vision. Kluwer, Dordrecht (1995)
25. Groemer, H.: Geometric Applications of Fourier Series and Spherical Harmonics. Cambridge University Press, New York (1996)
26. Guggenbuhl, P., Bodic, F., Hamel, L., Baslé, M.F., Chappard, D.: Texture analysis of X-ray radiographs of iliac bone is correlated with bone micro-CT. Osteoporos. Int. **17**(3), 447–454 (2006)
27. Guggenbuhl, P., Chappard, D., Garreau, M., Bansard, J.Y., Chales, G., Rolland, Y.: Reproducibility of CT-based bone texture parameters of cancellous calf bone samples: influence of slice thickness. Eur. J. Radiol. **67**(3), 514–520 (2008)
28. Hakulinen, M.A., Töyräs, J., Saarakkala, S., Hirvonen, J., Kröger, H., Jurvelin, J.S.: Ability of ultrasound backscattering to predict mechanical properties of bovine trabecular bone. Ultrasound Med. Biol. **30**(7), 919–927 (2004)
29. Helnwein, P.: Some remarks on the compressed matrix representation of symmetric second-order and fourth-order tensors. Comput. Methods Appl. Mech. Eng. **190**(22–23), 2753–2770 (2001)
30. Hollister, S., Kikuchi, N.: A comparison of homogenization and standard mechanics analyses for periodic porous composites. Comput. Mech. **10**(2), 73–95 (1992)
31. Hollister, S.J., Brennan, J.M., Kikuchi, N.: A homogenization sampling procedure for calculating trabecular bone effective stiffness and tissue level stress. J. Biomech. **27**(4), 433–444 (1994)

32. Homminga, J., Van Rietbergen, B., Lochmüller, E.M., Weinans, H., Eckstein, F., Huiskes, R.: The osteoporotic vertebral structure is well adapted to the loads of daily life, but not to infrequent "error" loads. Bone **34**(3), 510–516 (2004)

33. ÒHorn, B.K.P.: Extended Gaussian images. Proc. IEEE **72**(12), 1671–1686 (1984)

34. Ilic, S., Hackl, K., Gilbert, R.: Application of the multiscale FEM to the modeling of cancellous bone. Biomech. Model Mechanobiol. **9**(1), 87–102 (2010)

35. Jähne, B.: Digital Image Processing, 6th edn. Springer, Berlin (2005)

36. Jennane, R., Harba, R., Lemineur, G., Bretteil, S., Estrade, A., Benhamou, C.L.: Estimation of the 3D self-similarity parameter of trabecular bone from its 2D projection. Med. Image Anal. **11**(1), 91–98 (2007)

37. Jupp, P.E., Mardia, K.V.: A unified view of the theory of directional statistics, 1975–1988. Int. Stat. Rev. **57**(3), 261–294 (1989)

38. Kanatani, K.I.: Distribution of directional data and fabric tensors. Int. J. Eng. Sci. **22**(2), 149–164 (1984)

39. Keiner, J., Kunis, S., Potts, D.: Using NFFT 3—a software library for various nonequispaced fast Fourier transforms. ACM Trans. Math. Softw. **36**(4), 19:1–19:30 (2009)

40. Kim, C.H., Zhang, H., Mikhail, G., von Stechow, D., Müller, R., Kim, H.S., Guo, X.E.: Effects of thresholding techniques on microCT-based finite element models of trabecular bone. J. Biomech. Eng. **129**(4), 481–486 (2007)

41. Kinney, J.H., Stölken, J.S., Smith, T., Ryaby, J.T., Lane, N.: An orientation distribution function for trabecular bone. Bone **36**(2), 193–201 (2005)

42. Kleerekoper, M., Villanueva, A.R. Stanciu, J.: The role of three-dimensional trabecular microstructure in the pathogenesis of vertebral compression fractures. Calcif. Tissue Int. **37**(6), 594–597 (1985)

43. Klintström, E., Smedby, Ö., Moreno, R., Brismar, T.: Trabecular bone structure parameters from 3D image processing of clinical multi-slice and cone-beam computed tomography data. Skelet. Radiol. **43**(2), 197–204 (2014)

44. Knutsson, H.: Representing local structure using tensors. In: Proceedings of the Scandinavian Conference on Image Analysis (SCIA), Oulu, pp. 244–251 (1989)

45. Knutsson, H., Westin, C.F., Andersson, M.: Representing local structure using tensors II. In: Proceedings of the Scandinavian Conference on Image Analysis (SCIA), Ystad. Lecture Notes in Computer Science, vol. 6688, pp. 545–556 (2011)

46. Köthe, U., Felsberg, M.: Riesz-transforms versus derivatives: On the relationship between the boundary tensor and the energy tensor. In: Scale Space and PDE Methods in Computer Vision, Hofgeismar. Lecture Notes in Computer Science, vol. 3459, pp. 179–191 (2005)

47. Kreider, J.M., Goldstein, S.A.: Trabecular bone mechanical properties in patients with fragility fractures. Clin. Orthop. Relat. Res. **467**(8), 1955–1963 (2009)

48. Launeau, P., Robin, P.Y.F.: Fabric analysis using the intercept method. Tectonophysics **267**(1–4), 91–119 (1996)

49. Launeau, P., Archanjo, C.J., Picard, D., Arbaret, L., Robin, P.Y.F.: Two- and three-dimensional shape fabric analysis by the intercept method in grey levels. Tectonophysics **492**(1–4), 230–239 (2010)

50. Leng, K.D., Yang, Q.: Fabric tensor characterization of tensor-valued directional data: solution, accuracy, and symmetrization. J. Appl. Math. **2012**, 516,060–1–22 (2012)

51. Li, X., Yu, H.: Tensorial characterisation of directional data in micromechanics. Int. J. Solids Struct. **48**(14–15), 2167–2176 (2011)

52. Liu, Y., Saha, P.K., Xu, Z.: Quantitative characterization of trabecular bone micro-architecture using tensor scale and multi-detector CT imaging. In: Medical Image Computing and Computer-Assisted Intervention (MICCAI), Nice. Lecture Notes in Computer Science, vol. 7510, pp. 124–131 (2012)

53. Lofthag-Hansen, S.: Cone beam computed tomography radiation dose and image quality assessments. Swed. Dent. J. Suppl. (209), 4–55 (2009)

54. Lopes, R., Betrouni, N.: Fractal and multifractal analysis: a review. Med. Image. Anal. **13**(4), 634–649 (2009)

55. Majumdar, S., Lin, J., Link, T., Millard, J., Augat, P., Ouyang, X., Newitt, D., Gould, R., Kothari, M., Genant, H.: Fractal analysis of radiographs: assessment of trabecular bone structure and prediction of elastic modulus and strength. Med. Phys. **26**(7), 1330–1340 (1999)

56. Manenti, G., Capuani, S., Fanucci, E., Assako, E.P., Masala, S., Sorge, R., Iundusi, R., Tarantino, U., Simonetti, G.: Diffusion tensor imaging and magnetic resonance spectroscopy assessment of cancellous bone quality in femoral neck of healthy, osteopenic and osteoporotic subjects at 3T: preliminary experience. Bone **55**(1), 7–15 (2013)

57. Martin, R.B.: Toward a unifying theory of bone remodeling. Bone **26**(1), 1–6 (2000)

58. Mc Donnell, P., Liebschner, M., Tawackoli, W., Hugh, P.M.: Vibrational testing of trabecular bone architectures using rapid prototype models. Med. Eng. Phys. **31**(1), 108–115 (2009)

59. Millard, J., Augat, P., Link, T.M., Kothari, M., Newitt, D.C., Genant, H.K., Majumdar, S.: Power spectral analysis of vertebral trabecular bone structure from radiographs: orientation dependence and correlation with bone mineral density and mechanical properties. Calcif. Tissue Int. **63**(6), 482–489 (1998)

60. Mizuno, K., Matsukawa, M., Otani, T., Takada, M., Mano, I., Tsujimoto, T.: Effects of structural anisotropy of cancellous bone on speed of ultrasonic fast waves in the bovine femur. IEEE Trans. Ultrason. Ferroelectr. Freq. Control **55**(7), 1480–1487 (2008)

61. Moakher, M.: On the averaging of symmetric positive-definite tensors. J Elast **82**, 273–296 (2006)

62. Moreno, R., Borga, M., Smedby, O.: Estimation of trabecular thickness in gray-scale images through granulometric analysis. In: Proceedings of the SPIE Medical Imaging Conference 2012: Image Processing (SPIE), San Diego, vol. 8314, pp. 831451-1–831451-9 (2012)

63. Moreno, R., Borga, M., Smedby, Ö.: Evaluation of the plate-rod model assumption of trabecular bone. In: Proc of the International Symposium on Biomedical Imaging (ISBI), Barcelona, pp. 470–473 (2012)

64. Moreno, R., Borga, M., Smedby, Ö.: Generalizing the mean intercept length tensor for gray-level images. Med. Phys. **39**(7), 4599–4612 (2012)

65. Moreno, R., Borga, M., Klintström, E., Brismar, T., Smedby, Ö.: Correlations between fabric tensors computed on cone beam and microcomputed tomography images. In: Computational Vision and Medical Image Processing IV: VIPIMAGE 2013, Funchal. CRC, pp. 393–398 (2013)

66. Moreno, R., Pizarro, L., Burgeth, B., Weickert, J., Garcia, M.A., Puig, D.: Adaptation of tensor voting to image structure estimation. In: Laidlaw, D., Vilanova, A. (eds.) New Developments in the Visualization and Processing of Tensor Fields, pp. 29–50. Springer, Berlin (2012)

67. Mulvihill, B.M., Prendergast, P.J.: Mechanobiological regulation of the remodelling cycle in trabecular bone and possible biomechanical pathways for osteoporosis. Clin. Biomech. **25**(5), 491–498 (2010)

68. Naili, S., van Rietbergen, B., Sansalone, V., Taylor, D.: Bone remodeling. J. Mech. Behav. Biomed. Mater. **4**(6), 827–828 (2011)

69. Nazer, R.A., Lanovaz, J., Kawalilak, C., Johnston, J.D., Kontulainen, S.: Direct in vivo strain measurements in human bone-a systematic literature review. J. Biomech. **45**(1), 27–40 (2012)

70. Odgaard, A.: Three-dimensional methods for quantification of cancellous bone architecture. Bone **20**(4), 315–328 (1997)

71. Odgaard, A., Kabel, J., van Rietbergen, B., Dalstra, M., Huiskes, R.: Fabric and elastic principal directions of cancellous bone are closely related. J. Biomech. **30**(5), 487–495 (1997)

72. Ostoja-Starzewski, M.: Material spatial randomness: from statistical to representative volume element. Probab. Eng. Mech. **21**(2), 112–132 (2006)

73. Pahr, D.H., Zysset, P.K.: Influence of boundary conditions on computed apparent elastic properties of cancellous bone. Biomech. Model Mechanobiol. **7**(6), 463–476 (2008)

74. Parkinson, I.H., Fazzalari, N.L.: Methodological principles for fractal analysis of trabecular bone. J. Microsc. **198**(Pt 2), 134–142 (2000)

75. Pentland, A.P.: Fractal-based description of natural scenes. IEEE Trans. Pattern Anal. Mach. Intell. **6**(6), 661–674 (1984)

76. Perrot, C., Chevillotte, F., Panneton, R., Allard, J.F., Lafarge, D.: On the dynamic viscous permeability tensor symmetry. J. Acoust. Soc. Am. **124**(4), EL210–EL217 (2008)
77. Podsiadlo, P., Dahl, L., Englund, M., Lohmander, L.S., Stachowiak, G.W.: Differences in trabecular bone texture between knees with and without radiographic osteoarthritis detected by fractal methods. Osteoarthr. Cartil. **16**(3), 323–329 (2008)
78. Podshivalov, L., Fischer, A., Bar-Yoseph, P.Z.: 3D hierarchical geometric modeling and multiscale FE analysis as a base for individualized medical diagnosis of bone structure. Bone **48**(4), 693–703 (2011)
79. Riekkinen, O., Hakulinen, M., Lammi, M., Jurvelin, J., Kallioniemi, A., Töyräs, J.: Acoustic properties of trabecular bone—relationships to tissue composition. Ultrasound Med. Biol. **33**(9), 1438–1444 (2007)
80. van Rietbergen, B., Odgaard, A., Kabel, J., Huiskes, R.: Direct mechanics assessment of elastic symmetries and properties of trabecular bone architecture. J. Biomech. **29**(12), 1653–1657 (1996)
81. Rossi, C., Capuani, S., Fasano, F., Alesiani, M., Maraviglia, B.: DTI of trabecular bone marrow. Magn. Reson. Imaging **23**(2), 245–248 (2005)
82. Saha, P.K., Wehrli, F.W.: A robust method for measuring trabecular bone orientation anisotropy at in vivo resolution using tensor scale. Pattern Recognit. **37**(9), 1935–1944 (2004)
83. Saltykov, S.A.: Stereometric Metallography, 2nd edn. Metallurgizdat, Moscow (1958)
84. Schröder-Turk, G., Kapfer, S., Breidenbach, B., Beisbart, C., Mecke, K.: Tensorial Minkowski functionals and anisotropy measures for planar patterns. J. Microsc. **238**(1), 57–74 (2010)
85. Schröder-Turk, G.E., Mickel, W., Kapfer, S.C., Klatt, M.A., Schaller, F.M., Hoffmann, M.J.F., Kleppmann, N., Armstrong, P., Inayat, A., Hug, D., Reichelsdorfer, M., Peukert, W., Schwieger, W., Mecke, K.: Minkowski tensor shape analysis of cellular, granular and porous structures. Adv. Mater. **23**(22–23), 2535–2553 (2011)
86. Tabor, Z.: On the equivalence of two methods of determining fabric tensor. Med. Eng. Phys. **31**(10), 1313–1322 (2009)
87. Tabor, Z.: Equivalence of mean intercept length and gradient fabric tensors – 3d study. Med. Eng. Phys. **34**(5), 598–604 (2012)
88. Tabor, Z., Rokita, E.: Quantifying anisotropy of trabecular bone from gray-level images. Bone **40**(4), 966–972 (2007)
89. Varga, P., Zysset, P.K.: Sampling sphere orientation distribution: an efficient method to quantify trabecular bone fabric on grayscale images. Med. Image. Anal. **13**(3), 530–541 (2009)
90. Vasilić, B., Rajapakse, C.S., Wehrli, F.W.: Classification of trabeculae into three-dimensional rodlike and platelike structures via local inertial anisotropy. Med. Phys. **36**(7), 3280–3291 (2009)
91. Voyiadjis, G.Z., Kattan, P.I.: Advances in Damage Mechanics: Metals and Metal Matrix Composites with an Introduction to Fabric Tensors. Elsevier, Oxford (2006)
92. Wald, M.J., Vasilić, B., Saha, P.K., Wehrli, F.W.: Spatial autocorrelation and mean intercept length analysis of trabecular bone anisotropy applied to in vivo magnetic resonance imaging. Med. Phys. **34**(3), 1110–1120 (2007)
93. Wang, Q., Ronneberger, O., Burkhardt, H.: Rotational invariance based on Fourier analysis in polar and spherical coordinates. IEEE Trans. Pattern Anal. Mach. Intell. **31**(9), 1715–1722 (2009)
94. Whitehouse, W.J.: The quantitative morphology of anisotropic trabecular bone. J. Microsc. **101**(2), 153–168 (1974)
95. Winzenrieth, R., Michelet, F., Hans, D.: Three-dimensional (3D) microarchitecture correlations with 2D projection image gray-level variations assessed by trabecular bone score using high-resolution computed tomographic acquisitions: effects of resolution and noise. J. Clin. Densitom. **16**(3), 287–296 (2013)
96. Wolfram, U., Schmitz, B., Heuer, F., Reinehr, M., Wilke, H.J.: Vertebral trabecular main direction can be determined from clinical CT datasets using the gradient structure tensor and not the inertia tensor–a case study. J. Biomech. **42**(10), 1390–1396 (2009)

97. Wolski, M., Podsiadlo, P., Stachowiak, G.W.: Directional fractal signature analysis of trabecular bone: evaluation of different methods to detect early osteoarthritis in knee radiographs. Proc. Inst. Mech. Eng. H. **223**(2), 211–236 (2009)
98. Wolski, M., Podsiadlo, P., Stachowiak, G., Lohmander, L., Englund, M.: Differences in trabecular bone texture between knees with and without radiographic osteoarthritis detected by directional fractal signature method. Osteoarthr. Cartil. **18**(5), 684–90 (2010)
99. Xu, Z., Saha, P.K., Dasgupta, S.: Tensor scale: An analytic approach with efficient computation and applications. Comput. Vis. Image. Underst. **116**(10), 1060–1075 (2012)
100. Yang, G., Kabel, J., van Rietbergen, B., Odgaard, A., Huiskes, R., Cowin, S.C.: The anisotropic hooke's law for cancellous bone and wood. J. Elast. **53**(2), 125–146 (1998)
101. Yang, P.F., Brüggemann, G.P., Rittweger, J.: What do we currently know from in vivo bone strain measurements in humans? J. Musculoskelet. Neuronal. Interact. **11**(1), 8–20 (2011)
102. Yi, W.J., Heo, M.S., Lee, S.S., Choi, S.C., Huh, K.H.: Comparison of trabecular bone anisotropies based on fractal dimensions and mean intercept length determined by principal axes of inertia. Med. Biol. Eng. Comput. **45**(4), 357–364 (2007)
103. Zysset, P.K.: A review of morphology-elasticity relationships in human trabecular bone: theories and experiments. J. Biomech. **36**(10), 1469–1485 (2003)
104. Zysset, P., Curnier, A.: An alternative model for anisotropic elasticity based on fabric tensors. Mech. Mater. **21**(4), 243–250 (1995)